Industrial Health 2012, **50**, 103–114

Original Article

Flow and Containment Characteristics of an Air-curtain Fume Hood Operated at High Temperatures

Jia-Kun CHEN[1], Rong Fung HUANG[2]*, Pei-Yi HSIN[2], Ching Min HSU[1] and Chun-Wann CHEN[3]

[1] Graduate Institute of Applied Science and Technology, National Taiwan University of Science and Technology, Taipei, Taiwan, Republic of China

[2] Department of Mechanical Engineering, National Taiwan University of Science and Technology, 43 Keelung Road, Section 4, Taipei, Taiwan, Republic of China

[3] Institute of Occupational Safety and Health, Council of Labor Affairs, No. 99, Lane 407, Hengke Road, Shijr City, Taipei County, Taiwan, Republic of China

Received October 4, 2011and accepted December 21, 2011
Published online in J-STAGE February 1, 2012

Abstract: The flow and leakage characteristics of the air-curtain fume hood under high temperature operation (between 100°C and 250°C) were studied. Laser-assisted flow visualization technique was used to reveal the hot plume movements in the cabinet and the critical conditions for the hood-top leakage. The sulfur hexafluoride tracer-gas concentration test method was employed to examine the containment spillages from the sash opening and the hood top. It was found that the primary parameters dominating the behavior of the flow field and hood performance are the sash height and the suction velocity as an air-curtain hood is operated at high temperatures. At large sash height and low suction velocity, the air curtain broke down and accompanied with three-dimensional flow in the cabinet. Since the suction velocity was low and the sash opening was large, the makeup air drawn down from the hood top became insufficient to counter act the rising hot plume. Under this situation, containment leakage from the sash opening and the hood top was observed. At small sash opening and high suction velocity, the air curtain presented robust characteristics and the makeup air flow from the hood top was sufficiently large. Therefore the containment leakages from the sash opening and the hood top were not observed. According to the results of experiments, quantitative operation sash height and suction velocity corresponding to the operation temperatures were suggested.

Key words: Air-curtain fume hood, Flow visualization, Tracer-gas test, High temperature operation

Introduction

Fume hoods are ventilated enclosures widely used in laboratories to protect users far from the hazardous components in chemical and biological works. An exhaust system is connected to the fume hood that draws room air through the hood's sash opening and ejects the mixture of contaminated air out of the laboratory. The structures of fume hoods have not changed appreciably over sixty years[1, 2]. Previous studies[3–9] suggested that maintaining a specific face velocity does not assure that a fume hood contains hazardous chemical fumes and vapors. The boundary layer separation and flow recirculation induced by the flow/hood

*To whom correspondence should be addressed.
E-mail: rfhuang@mail.ntust.edu.tw

structure interaction and formed around the doorsill, the sash, and the side posts of fume hoods were the primary potential hazard of containment spillage[10–13]. The presence of the operator might also induce a large recirculation bubble around his chest because the flow drawn into the sash opening goes across the operator's body which can be considered as a situation of bluff-body in crossflow[10–14]. Investigators acknowledged the leakage problem of the fume hood and many methods have been proposed to improve the hood performance based on the conventional fume hood structure, for instance, the by-pass design inside the hood above the sash, the auxiliary air near the face of the hood just above the worker, the doorsill airfoil installation, the doorsill compensation air, the variable air volume (VAV) operation[15], the adaptive back baffle for sash vortex manipulation (the Bi-stable Vortex Hood), and the vortex-isolation technique (the Berkeley Hood), etc.

The air-curtain fume hood (AC Hood) recently proposed by Huang *et al*.[16, 17] has been proved to be effective in preventing containment leakage of the fume hood for both the static and dynamic situations. The air-curtain fume hood is an advanced industrial product. Many sets have been installed in the laboratories of university and research institutes in Taiwan. Due to its specific aerodynamic design, the air-curtain fume hood has extremely high containment performance with drastically low suction flow rate and noise when compared with the conventional fume hoods[16, 17]. Its abilities of resisting the influences of people walk-by and cross draft are particularly significant. Huang *et al*.[18] employed the push-pull technique to setup a stable "two-dimensional" air curtain across the sash opening of a fume hood. A "planar jet" was installed across the bottom of the sash and a suction slot was arranged on the work surface and just behind the doorsill. Makeup air was allowed to flow into the hood through the grid or screen ceiling as the suction applied. By properly adjusting the velocities of the push jet and the suction flow, the flow resistance of the grid ceiling, and the hood geometries, a robust air curtain was formed across the sash opening. The air-curtain hood can attain a performance of less than 0.001 ppm of SF_6 concentration leakage by using the EN-14175[19] and ANSI/ASHRAE-110[20] protocols. Their examinations on the flow field found no recirculation flows in the cabinet. From the point of view of the aerodynamics and mass transport, the results indicated that the air curtain properly setup across the sash opening allows almost no sensible exchange of momentum and mass between the pollutants in the cabinet and the air of the environment. Tsai *et al*.[21, 22] evaluated the airborne nanoparticle exposures while nanoparticles were handled in a constant-flow fume hood, a constant-velocity fume hood, and an air-curtain fume hood. They reported that the use of the conventional fume hood for nanoparticle handling must be approached with caution, since particles escaped from conventional hoods could be substantial and the magnitude of the release depended on various conditions of use. A worker's arm motions, if energetic, induced strong turbulence which worked with the complex vortex inside the hood to carry nanoparticles to the worker's breathing zone. The performance of the air-curtain fume hood contributed to nanoparticle use was outstanding for various conditions, and avoided the difficulties found when using conventional hoods.

Since the top of the air-curtain fume hood was installed with a grid or screen in order to allow the makeup air to flow into the hood cabinet as the suction was applied, a safety problem may be induced in case the contaminant fumes are released under high temperature operation from a heat source. In order to examine the leakage problem which may be caused by the high temperature operation of the air-curtain hood, experiments of placing an oil pan on a hot plate heated to a temperature between 180 and 300°C were conducted. The mineral oil in the heated pan generated large amount of oil vapor and rose up. Laser-assisted flow visualization was employed to identify the maximum height the oil vapor attained as the air-curtain hood was operated at various suction velocities. The tracer-gas (SF_6) concentration detection method was used to examine the leakage level from the sash opening when a SF_6 ejector was placed on the hot plate.

Materials and Methods

Air-curtain fume hood

The air-curtain hood used in the study was similar to the one discussed by Huang *et al*[16]. It was summarized briefly here. Figure 1 shows the front and side views of the air-curtain fume hood. Important dimensions were noted in the figure. The hood consisted of three main parts – (1) a double-layered sash structured for supply of push jet with a velocity v_b, (2) a suction slot installed behind the doorsill for exhaust of contaminants with a suction velocity v_s, and (3) a cabinet with screens or perforated plates installed on the top. The top of the cabinet was covered by mesh screens or perforated plates so that the air could be drawn into the cabinet by natural convection due to the suction applying at the suction slot. The push jet and the suction flow were designed to create an air curtain[18] on the sash plane to aerodynamically separate the interior of the

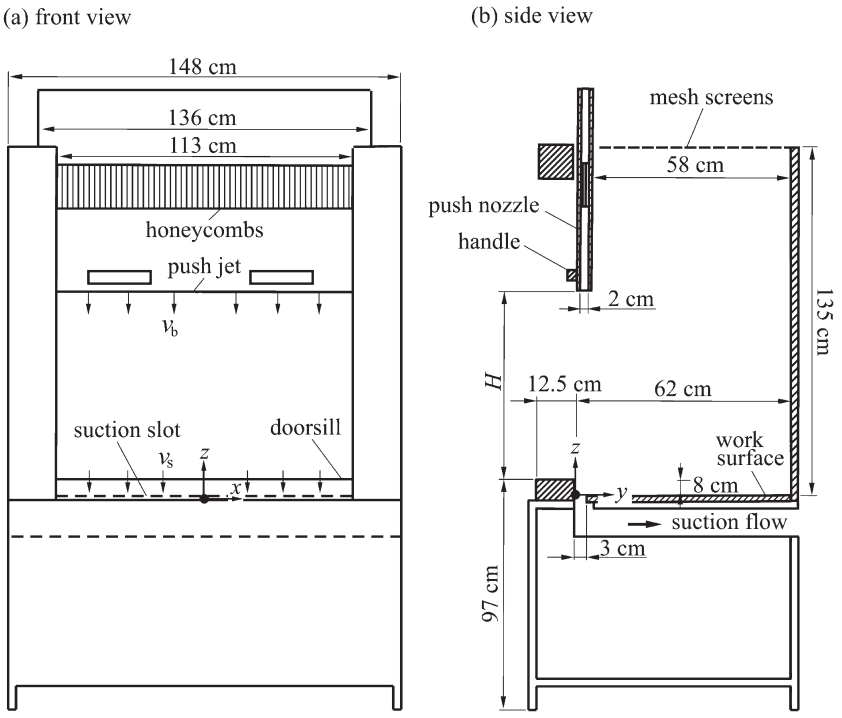

Fig. 1. Hand sketches of air-curtain fume hood used for study.

cabinet from the outside atmosphere. The fume hood was made of plexiglas which allowed the laser-light sheet to penetrate so that flow visualization became possible. The suction flow was driven by a centrifugal fan and the push jet was supplied by several crossflow fans. Inverters and Venturi flow meters were used to control the flow speeds and to measure the flow rates, respectively. The Venturi flow meters were equipped with high precision pressure transducers which were constantly calibrated in house. The accuracy of the flow rate measurement was within the range of 1.5% of converted reading. The coordinate system and the geometric dimensions were designated in the figure. The dimensions of the inner work space inside the cabinet were 146 cm (lenth) × 62 cm (width) × 135 cm (height). The exit dimensions of the push jet were 120 cm (length) × 2 cm (width). The suction slot was a narrow rectangular opening with 3 cm in width and 120 cm in length.

Flow visualization

When the flow visualization experiments were conducted, an oil pan with a diameter of 28 cm was placed on the hot plate of an electric heater which was installed on the work surface of the hood. The mineral oil with a boiling temperature of about 280°C was filled to the pan. During the experiments, the temperatures of the hot plates (T_{plate}) were set between 180°C and 300°C and the temperature of the oil (T_{oil}) contained in the pan was between 140°C and 240°C. Large amounts of hot oil mists were generated and rose from the heated oil pan for flow visualization. The diameter of the oil mist particles, measured by means of a particle analyzer (Model 2600C, Malvern Instrument Ltd., Malvern, Worcestershire, UK), was 1.7 ± 0.2 μm. The density was 0.821 g/ml. Ignoring the effect of turbulent diffusion, the relaxation time constant was estimated to be less than 7.7×10^{-5} sec and the Stokes number was on the order of 10^{-6} within the range of experiment. Therefore, the seeding particles could properly follow the flow fluctuations at least up to 10 kHz[23]. A laser beam, provided by a 100 mW Nd-YAG, passed through a laser-light expander to form a laser-light sheet. The thickness of the laser-light sheet was 0.5 mm. The visualizations were performed by arranging the laser-light sheet in the horizontal and vertical planes. The oil mist scattered the laser light and made the images of the mist in the plane of the laser-light sheet clearly visible. The images of oil mist in the laser-light sheet were recorded by a charge-coupled device (CCD) camera. The camera can record images at 30 frames per second. The exposure time used in the study was 1/60. Experiments were carried out in a well-controlled test

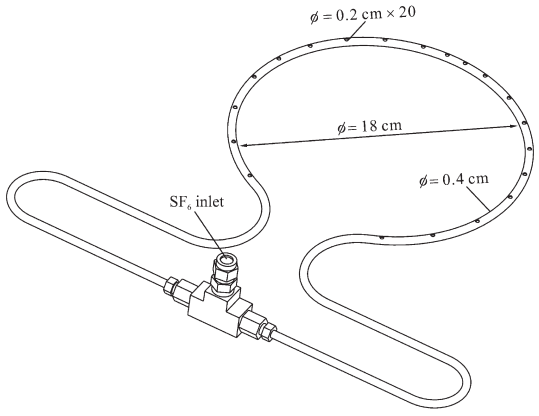

Fig. 2. Gas-releasing ring for SF_6 concentration measurement.

room. The test room was a typical laboratory room with dimensions of 19 m (length) × 16 m (width) × 5 m (height). During the experiment, turbulence and interference from external sources such as air supply diffusers, doors, and traffic in the room were restricted.

Tracer gas tests

The SF_6 (sulfur hexafluoride) tracer-gas concentration detection method was employed to evaluate the leakage level of the hood from the sash opening by simulating the EN 14175-3 protocol with slight modification for tests at the sash height H=25 and 50 cm. 10% of SF_6 in N_2 was released from small holes in a homemade gas release ring shown in Fig. 2. The gas release ring was made of copper tube with an outer diameter of 0.4 cm. In total, 20 small holes with diameters of 0.2 cm were drilled along each gas release ring to eject SF_6 gas. A pressure gauge, a needle valve, and a rotameter calibrated with the SF_6/N_2 mixture were attached to a piping system to control the flow rate of SF_6. The flow rate of SF_6, Q_{SF6}, released from the gas release ring was 2 l/min. The exit velocity of SF_6 from the ejecting holes was thus about 0.33 m/s. When the experiments were conducted, the gas release ring was placed on the hot plate (24 cm in diameter) of the electric heaters in order to receive the heat and buoyancy from the hot plate.

Nine sampling probes were arranged in a grid based on a square area of 20 cm × 20 cm, as shown in Fig. 3. The sampling probes were connected to the inlets of a mixing manifold by Teflon tubes of equal length. The detector probe was affixed to the outlet of the mixing manifold. Each sampling probe had a funnel-shaped effuser with a 3-cm inner diameter at the inlet of the probe. Each funnel-shaped effuser was fitted to a stainless steel tube with an inner diameter of 0.5 cm and a length of 15 cm. The

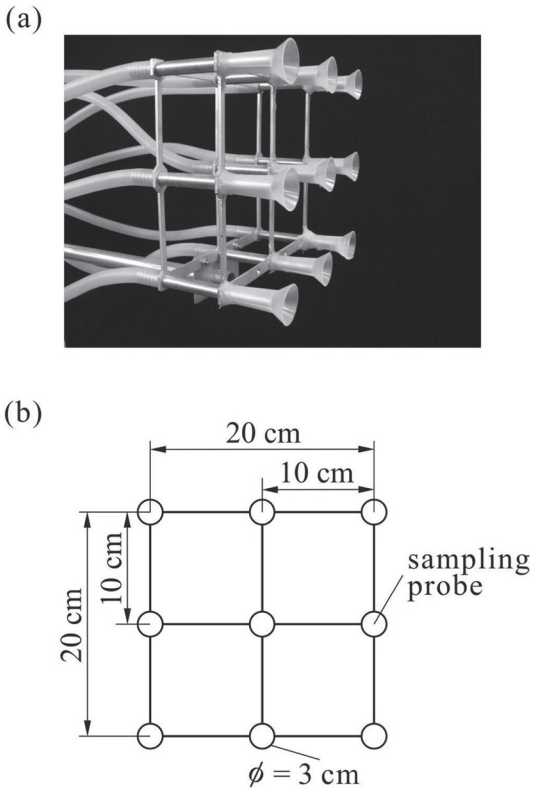

Fig. 3. Grid of sampling probe for SF_6 concentration measurement across sash opening.
(a) picture, (b) grid dimension.

suction velocity at the inlet of the funnel-shaped effuser was approximately 4 cm/s. The sampling probes were placed at the locations P1–P3 (upper raw) and P4–P6 (lower raw) shown in Figs. 4(a) and (b) as the sash height H=50 cm and the locations P1–P3 shown in Fig. 4(c) as the sash height H=25 cm to evaluate the local averaged and maximum values of SF_6 concentration detected in the plane of sash opening. The detected SF_6 concentrations may provide information regarding the leakages from the sash opening. The face of the funnel-shaped-effuser inlets was placed on the plane y=0.

A Miran SapphIRe™ Infrared Analyzer (Thermo Electron Corp., Franklin, Massachusetts, USA) was used to measure the concentration of SF_6 gas. The lower and upper limits of SF_6 concentration that the instrument can detect were 0.001 ppm and 100 ppm, respectively. The resolution was 0.001 ppm. The instrument was calibrated in house. The internal sampling rate of the detector was 20 readings per second. Averaged readings over 1 s were recorded as one data point so that each recorded datum represented an average of 20 readings sampled in 1 s. For each measurement, the data of SF_6 concentration were continuously

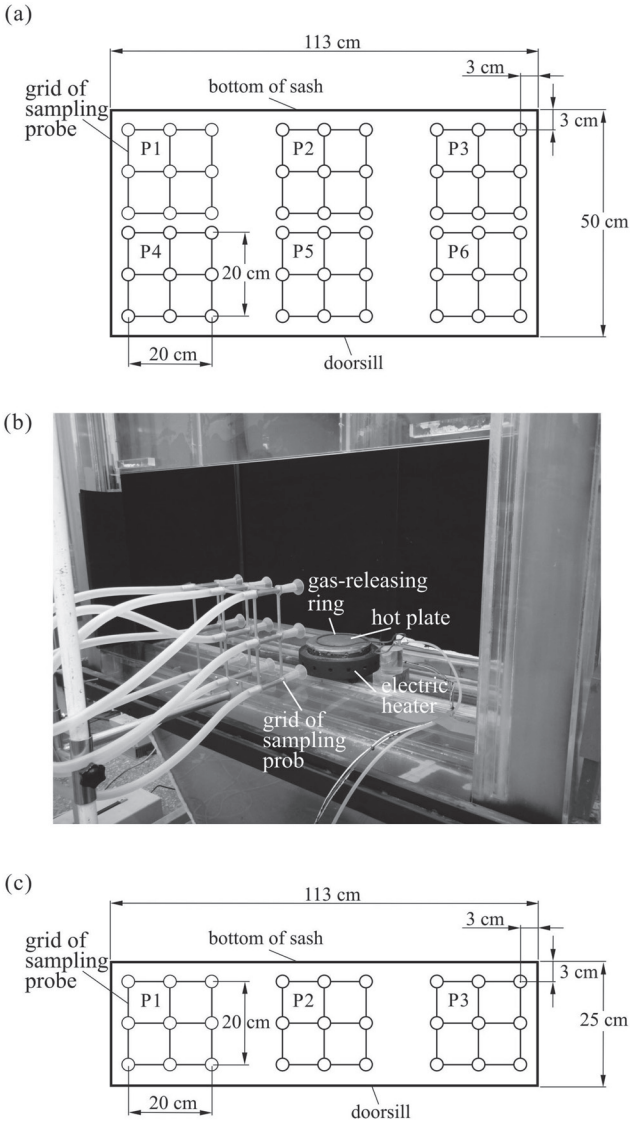

Fig. 4. Allocation of sampling grid for SF_6 concentration measurement across sash opening.
(a) deployment of sampling grid at sash height H=50 cm, (b) picture of installation, (c) deployment of sampling grid at sash height H=25 cm.

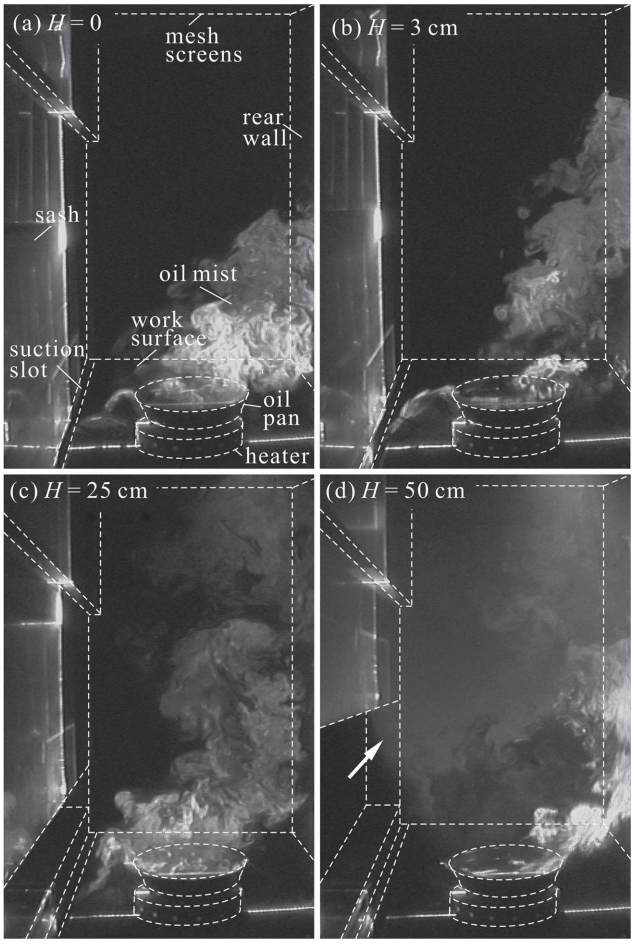

Fig. 5. Flow visualization images of hot plume in symmetry plane x=0.
v_s=6 m/s, v_b=1 m/s, T_{plate}=240°C, T_{oil}=220°C. H=(a) 0, (b) 3 cm, (c) 25 cm, (d) 50 cm.

recorded while the tracer gas was released into the cabinet for 360 s; that is, 360 data points were obtained from 7,200 readings. Mean and peak values of SF_6 concentration data were calculated over the recorded data. The data recorded in the initial period of 59 s was discarded.

The SF_6 tracer-gas concentration detection method was also employed to evaluate the quantitative level of SF_6 leaking from the hood top in order to examine the correlations between the quantitative measurements with the flow visualization results under the high temperature operation condition. When these experiments were performed, the detector probe of the Miran SapphIRe™ Infrared Analyzer was installed at a location 1 cm above the hood top with the center of the suction probe inlet at (x, y, z)=(0, 59, 136) cm to measure the SF_6 concentration leaking from the hood top. The elapsed time for measurement of the hood-top leakage was 6 min after the SF_6 gas was ejected from the gas-releasing ring which was placed on the hot plate. The data from the beginning of the second minute to the end of the sixth minute were used for average.

Results and Discussion

Flow visualization

Figure 5 shows the oil mist images in the symmetry plane at various sash height. The hot plate and oil temperatures are T_{plate}=240°C and T_{oil}=220°C, respectively. The suction and blow velocities which are used to form the air curtain across the sash opening are v_s=6 m/s and v_b=1

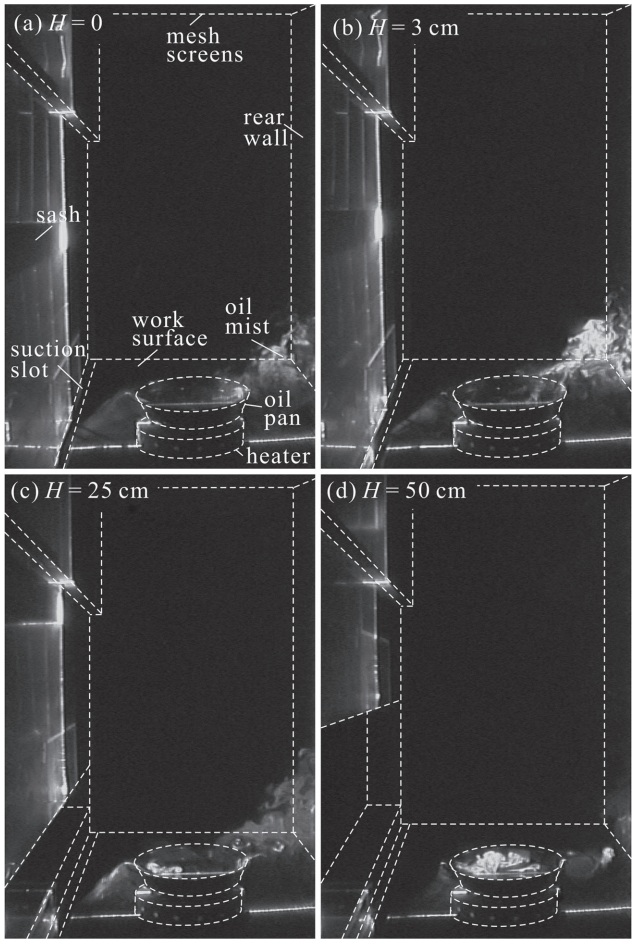

Fig. 6. Flow visualization images of hot plume in symmetry plane *x*=0.

v_s=12 m/s, v_b=1 m/s, T_{plate}=240°C, T_{oil}=220°C. *H*=(a) 0, (b) 3 cm, (c) 25 cm, (d) 50 cm.

m/s, respectively. As the sash is closed (Fig. 5(a)), strong turbulence is induced by the counter action between the buoyancy and the downward flow. Oil mist near the rear wall rises up to about half height of the cabinet. Therefore, no danger of leakage from the hood top is observed. As the sash is open to *H*=3 cm (Fig. 5(b)), oil mist near the rear wall rises up to a height about three quarter of the cabinet height. Occasionally the turbulent flow brings the oil mist to the hood top. At *H*=25 and 50 cm as shown in Fig. 5(c) and Fig. 5(d) respectively, the oil mist rises up beyond the hood top. In Fig. 5(d), the oil mist tumbles and swirls in the whole cabinet. Some oil mist even goes through the sash opening as indicated by the arrow.

Figure 6 shows the oil mist images in the symmetry plane of the hood at various sash height as the suction and jet velocities are operated at v_s=12 m/s and v_b=1 m/s respectively. The hot plate and oil temperatures are the same as those of Fig. 5, i.e., T_{plate}=240°C and T_{oil}=220°C. Due to the increase of the suction velocity, major part of the oil mist rises from the heated oil pan is inhaled into the suction slot installed behind the doorsill for all sash height. A little trace of oil mist in the lower part of the cabinet near the rear wall is observed. No leakage of oil mist from sash opening is found. Apparently, at v_s=12 m/s, the buoyancy effect induced by the high temperature operation does not cause breakdown of the hood performance even when the sash is open to *H*=50 cm.

Figure 7 shows the oil mist images observed in the horizontal plane *z*=28 cm. At *H*=25 cm and v_s=6 m/s (Fig. 7(a)), some of the oil mist disperse to the left rear part of the cabinet. Three-dimensional flow must be formed at such a small suction velocity and low sash height. At *H*=25 cm and v_s=12 m/s (Fig. 7(b)), no dispersion of the oil mist to the left and right of the cabinet. The hot plume rises up a little (as seen in Fig. 6(c)) without disperses laterally. At *H*=50 cm and v_s=6 m/s (Fig. 7(c)), the oil mist spreads in the whole horizontal plane. By combining the observations of Fig. 5(d) and Fig. 7(c), it is apparent that at large sash opening *H*=50 cm and low suction velocity v_s=6 m/s, the hot plume induces serious three dimensional flow in the cabinet. Under this situation, leakages of containments from the hood top and the sash opening are expected. At *H*=50 cm and v_s=12 m/s (Fig. 7(d)), some oil mist disperse toward the rear part of the cabinet. Some three-dimensional flow must be formed. However, by combining the observations of Fig. 6(d) and Fig. 7(d), the oil mist does not go up far from the oil pan and does not disperse toward the sash opening. Most of the dispersed oil mist is restricted in the area around the lower cabinet near the rear wall. From the observations of Figs. (5), (6), and (7), it is understood that higher suction velocity and smaller sash height help the flows in the cabinet to present more features of two dimensionality. Small suction velocity and large sash height may induce serious three-dimensional flow problem in the cabinet and containment leakage out of the hood top and sash opening.

The behavior of the air curtain under the high temperature operation was examined by injecting the mist of mineral oil into the push nozzle of the double-layered sash. The home-made smoke generator was used to provide the smokes. Figure 8 shows the traces of the jet fluids issued from the double-layered sash. The jet velocity was v_b=1 m/s. The oil pan was not installed on the hot-plate of the electric heater, while the hot plate was heated to T_{plate}=300°C. The traces of the smokes show the images of the air curtain. The air curtains in Figs. 8(a), (c), and (d) for (*H*,

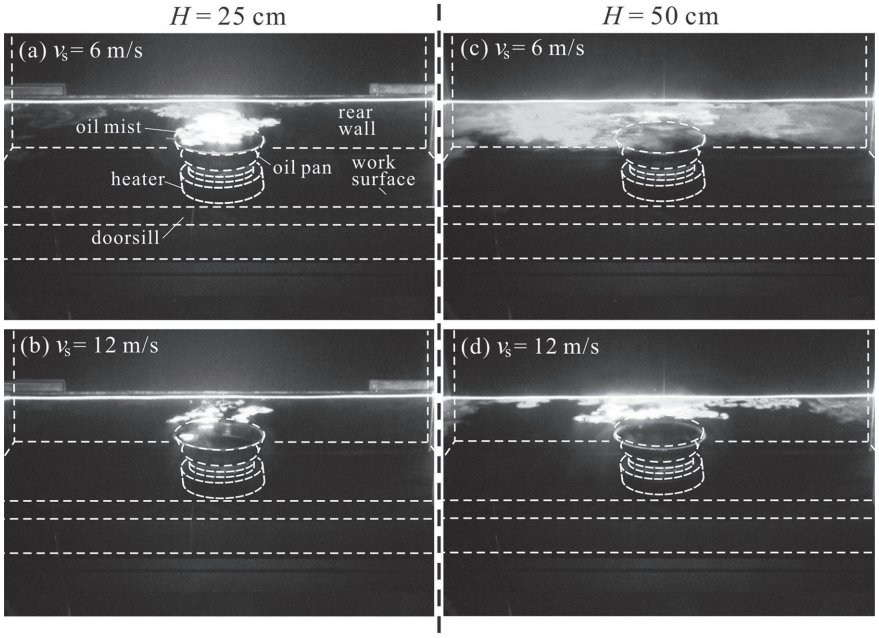

Fig. 7. Flow visualization images of hot plume in horizontal plane z=28 cm.
T_{plate}=240°C, T_{oil}=220°C, v_b=1 m/s. (H, v_s)=(a) (25 cm, 6 m/s), (b) (25 cm, 12 m/s), (c) (50 cm, 6 m/s), (d) (50 cm, 12 m/s).

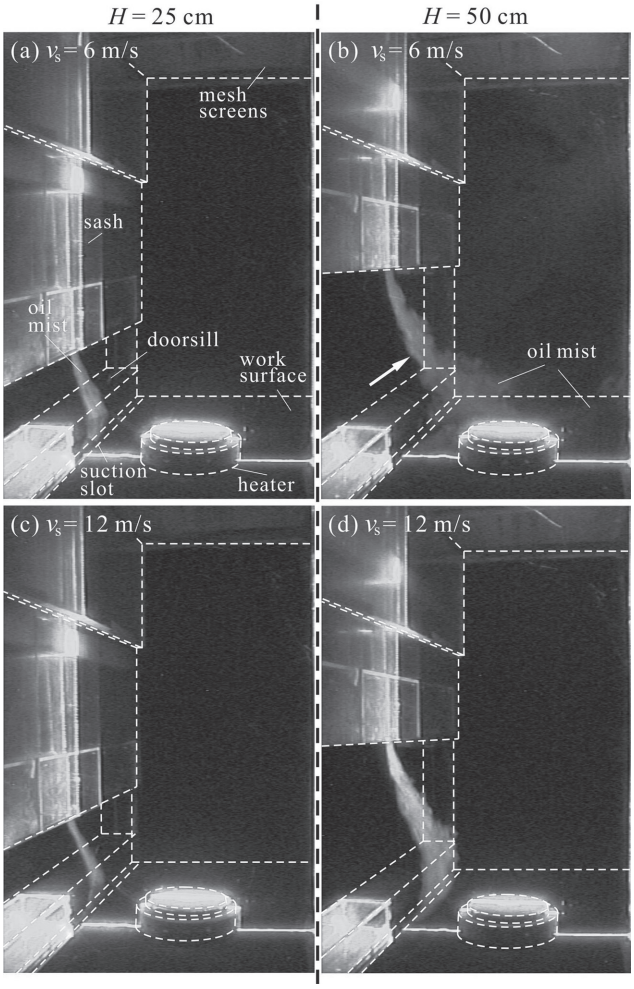

v_s)=(25 cm, 6 m/s), (25 cm, 12 m/s), and (50 cm, 12 m/s), respectively, present slightly concave mode[16], which the air curtains are pushed inwards the cabinet slightly by the air inhaled from the outside atmosphere before they direct into the suction slots. Negligible containment leakage from the sash opening was detected as an air-curtain fume hood was operated at this characteristic flow mode at regular operation temperatures[16]. The hot plume images shown in Figs. 5(c), 6(c), and 6(d), which correspond to the situations of the air curtains shown in Figs. 8(a), 8(c), and 8(d), show no traces of oil mist releasing through the sash opening. At large sash opening H=50 cm and low suction velocity v_s=6 m/s, as shown in Fig. 8(b), the air curtain presents severely concave mode—lots of the jet fluids is entrained into the cabinet and curve up to form a vortex. The vortical flow is easily observed in Fig. 5(d). Under this situation, the containment leakage happens easily through the hood top and the sash opening, as indicated in Fig. 5(d).

Maximum height of oil mist

The movements of hot oil-mist plume recorded in the movies were examined. The maximum height the hot

Fig. 8. Flow visualization images of air curtain in symmetry x=0.
T_{plate}=300°C, v_b= 1 m/s. (H, v_s)=(a) (25 cm, 6 m/s), (b) (25 cm, 12 m/s), (c) (50 cm, 6 m/s), (d) (50 cm, 12 m/s).

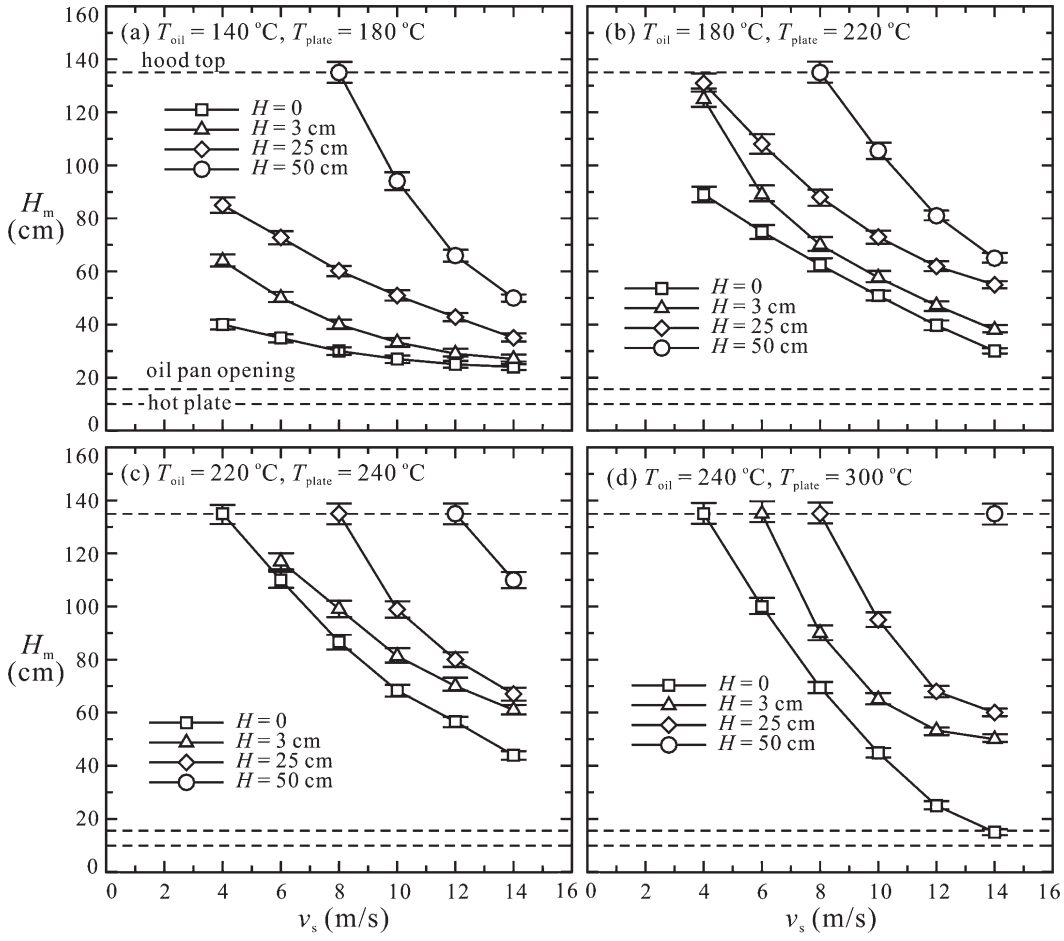

Fig. 9. Maximum height hot plume attains in symmetry plane x=0.
v_b=1 m/s. (T_{plate}, T_{oil})=(a) (140, 180) °C, (b) (180, 220) °C, (c) (220, 240) °C, (d) (240, 300) °C. Maximum uncertainties associated with error bars: ± 3% of reading.

plume attains within five minutes recorded in the movie was evaluated. Figure 9 shows the maximum height H_m in the symmetry plane (x=0) the plume attains at various sash height H as the suction velocity v_s varies. The dashed lines marked from top to bottom of Fig. 9 denote the locations of the hoot top, oil pan opening, and hot plate. At the oil temperature T_{oil}=140°C (Fig. 9(a)) and 180°C (Fig. 9(b)), the maximum height H_m the hot plume attains never exceeds half cabinet height if the sash height H is set below 25 cm and the suction velocity is larger than 8 m/s. If the sash height H=50 cm, the suction velocity v_s has to be larger than about 12 m/s so that the maximum hot plume height H_m attains below half cabinet height. At the oil temperature T_{oil}=220°C (Fig. 9(c)) and 240°C (Fig. 9(d)), the hot plume never exceeds half cabinet height if the sash height H is set below 25 cm and the suction velocity is larger than 12 m/s. If the sash height H=50 cm, it is difficult to avoid leakage of hot plume from the hood top even though the suction velocity v_s is increased beyond 14 m/s. Huang *et al*[16]. suggested to operate the air-curtain fume hood at a suction velocity v_s>8 m/s at the regular temperature operations if negligible containment leakage is desired. From the results of the present study shown in Figs. 9(a) and (b), it is suggested that if the operation temperature is between 100°C and 200°C the sash height H has to be smaller than 25 cm in order to maintain the criteria of minimum suction velocity v_s =8 m/s. If the sash height is 50 cm, however, the suction velocity has to increase to values beyond 12 m/s to confine the hot plume below the half cabinet height. From the results of Figs. 9(c) and (d), it is suggested that if the operation temperature is between 200°C and 250°C the sash height should not be larger than 25 cm and the suction velocity should not be less than 12 m/s.

Figure 10 shows the maximum height H_m obtained from the flow visualization results in the off set plane x=14 cm

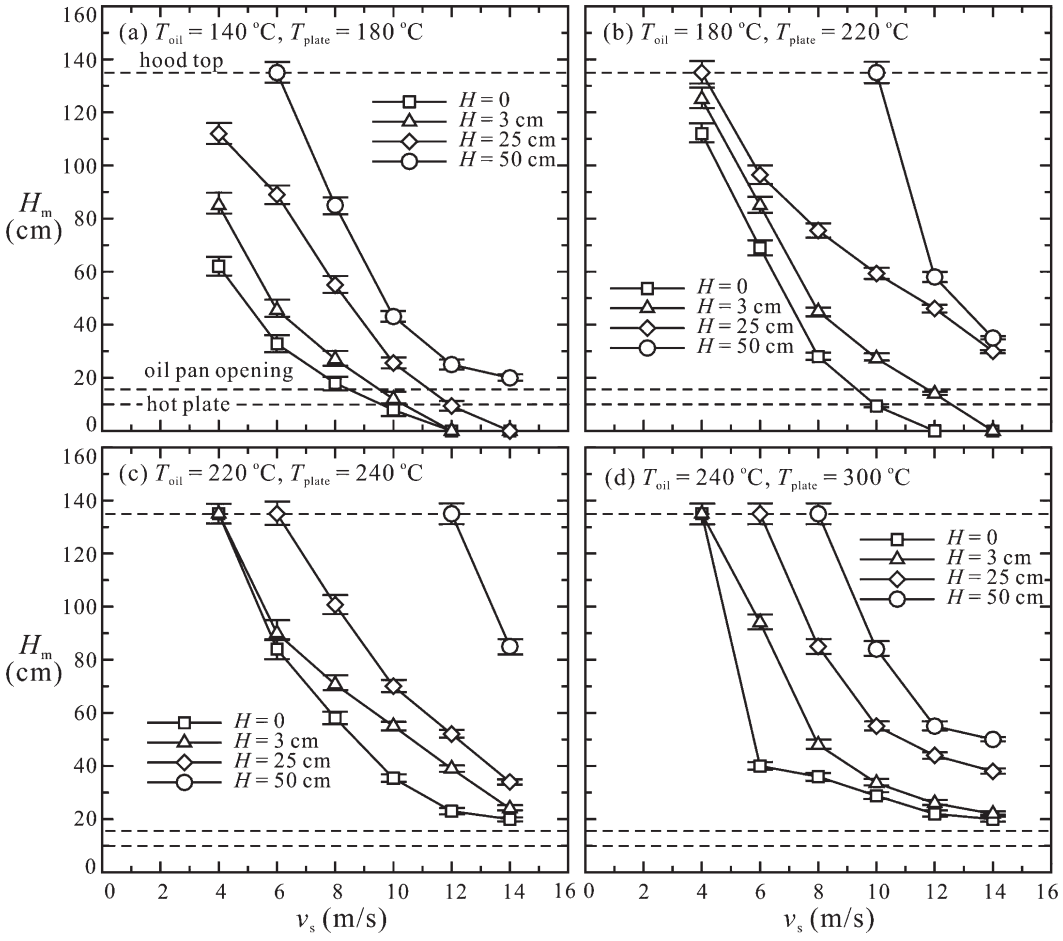

Fig. 10. Maximum height hot plume attains in off-set plane x=14 cm.
v_b=1 m/s. (T_{plate}, T_{oil})=(a) (140, 180) °C, (b) (180, 220) °C, (c) (220, 240) °C, (d) (240, 300) °C. Maximum uncertainties associated with error bars: ± 3% of reading.

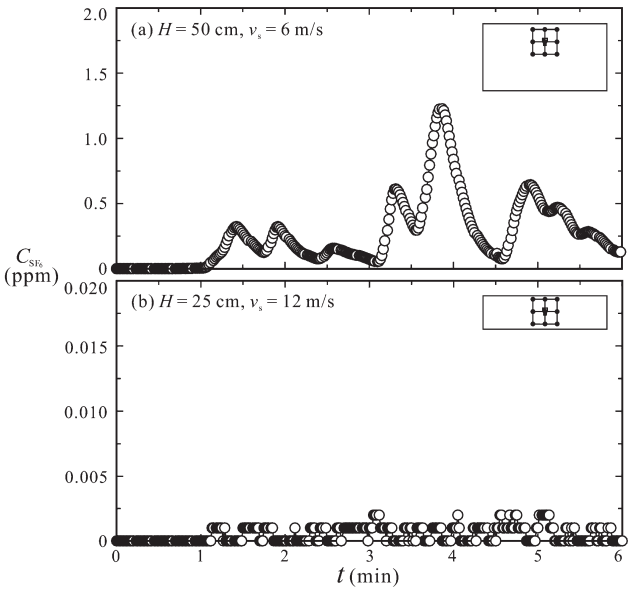

at various sash height H as the suction velocity v_s varies. The phenomena are similar to those of Fig. 9—smaller sash height and larger suction velocity benefit high temperature operation. The slopes of the curves in Fig. 10 are not the same as those in Fig. 9 because of the influence of three-dimensional flows and turbulence, the suggestions for safe operation at elevated temperatures are the same.

Tracer-gas concentration leakage across sash opening and hood top

Typical time histories of the tracer-gas concentration measurements across the sash opening are shown in Fig. 11. In Fig. 11(a), the sampling probe is placed at the location P2 of Fig. 4(a). The sash height and the suction velocity are 50 cm and 6 m/s, respectively. The measured

Fig. 11. Typical time histories of measured concentrations of SF_6 tracer gas across sash opening.
T_{plate}=220°C. (H, v_s)= (a) (50 cm, 6 m/s), (b) (25 cm, 12 m/s).

Table 1. Averaged SF_6 concentrations detected across sash opening under various operation conditions

v_s (ms^{-1})	Sampling grid location	C_{ave} (ppm)			
		T_{plate} = 180°C	T_{plate} = 220°C	T_{plate} = 260°C	T_{plate} = 300°C
6	P1	0.001	0.003	0.003	0.005
	P2	0.002	0.003	0.002	0.008
	P3	0.002	0.003	0.005	0.003
8	P1	0.001	0.002	0.002	0.003
	P2	0.001	0.001	0.002	0.004
	P3	0.001	0.003	0.003	0.002
10	P1	<0.001	0.001	0.001	0.001
	P2	0.001	0.001	0.001	0.002
	P3	0.001	0.001	0.001	0.001
12	P1	<0.001	0.001	<0.001	0.001
	P2	<0.001	0.001	0.001	<0.001
	P3	0.001	0.001	<0.001	<0.001

H=25 cm, v_b=1 ms^{-1}.

Table 2. Averaged SF_6 concentrations detected across sash opening under various operation conditions

v_s (ms^{-1})	Sampling grid location	C_{ave} (ppm)			
		T_{plate} = 180°C	T_{plate} = 220°C	T_{plate} = 260°C	T_{plate} = 300°C
6	P1	0.133	0.238	0.411	0.661
	P2	0.058	0.321	0.391	0.724
	P3	0.103	2.050	0.900	3.979
	P4	0.098	0.448	0.930	3.889
	P5	0.046	0.480	1.302	3.483
	P6	0.052	1.060	2.131	2.555
8	P1	0.018	0.031	0.013	0.258
	P2	0.031	0.025	0.032	0.082
	P3	0.013	0.023	0.051	0.586
	P4	0.030	0.021	0.410	0.556
	P5	0.025	0.014	0.241	0.053
	P6	0.026	0.018	0.487	0.530
10	P1	0.008	0.009	0.007	0.015
	P2	0.010	0.007	0.014	0.013
	P3	0.008	0.014	0.004	0.004
	P4	0.019	0.020	0.003	0.015
	P5	0.013	0.008	0.014	0.006
	P6	0.025	0.014	0.013	0.021
12	P1	0.004	0.005	0.003	0.006
	P2	0.011	0.001	0.004	0.006
	P3	0.007	0.006	0.003	0.001
	P4	0.014	0.009	0.001	0.001
	P5	0.008	0.003	0.011	0.002
	P6	0.014	0.007	0.003	0.005

H=50 cm, v_b=1 ms^{-1}.

Table 3. Results of SF_6 tracer-gas concentration detected across sash opening of a conventional fume hood at a regular operation temperature 26°C

Hood type	Sampling grid position	C_{ave} (ppm)	C_{max} (ppm)
Conventional fume hood	P1	0.021	0.052
	P2	0.081	0.151
	P3	0.032	0.063
	P4	23.963	45.881
	P5	27.371	51.834
	P6	30.534	43.522

H=50 cm, Q_s=0.36 m^3s^{-1}. Cited from previous study reported by Huang *et al*[16].

SF_6 concentration leaking out of the sash opening fluctuates drastically as the time evolves. The maximum leakage may attain about 1.25 ppm. This phenomenon corresponds to the results of flow visualization shown in Fig. 5(d). In Fig. 11(b), the sampling probe is placed at the location P2 of Fig. 4(c). The sash height and the suction velocity are 25 cm and 12 m/s. Under this situation, the measured SF_6 concentrations are negligible small. The maximum value may be as low as 0.002 ppm, which corresponds to the flow visualization results shown in Fig. 6(c).

Table 1 shows the averaged SF_6 concentrations measured at the locations P1, P2, and P3 shown in Fig. 4(c) for H=25 cm. It is apparent that at H=25 cm all SF_6 concentration measurements present negligibly small values (less than 10 ppb) for all of the high temperature operations from T_{plate}=180°C to 300°C. Table 2 shows the averaged SF_6 concentrations detected at the locations P1–P6 shown in Fig. 4(a) for H=50 cm. As the suction velocity is 6 m/s, the order-of-magnitude of the detected maximum SF_6 concentrations is about $O(1)$. At v_s=8 m/s, the order-of-magnitude of the detected maximum SF_6 concentrations becomes about $O(10^{-1})$. As the suction velocity attains 10 and 12 cm/s, the order-of-magnitude of the detected maximum SF_6 concentrations decreases to about $O(10^{-2})$. For comparison, previous data obtained by Huang *et al*[16]. for regular temperature operation at about 26°C is shown in Table 3. The detected maximum averaged SF_6 may attain about 30 ppm which corresponds to an order-of-magnitude of $O(10^2)$. The air-curtain fume hood, even though operated at elevated temperature condition, present high containment performance.

Table 4 shows the SF_6 concentration measured at the location 1 cm above the hood top at T_{oil}=180°C and T_{plate}=220°C. At H=3 cm, C_{ave} of the SF_6 concentration is 0.001 ppm at V_s=4 m/s. While at higher suction velocities

Table 4. Averaged SF_6 concentrations measured at location 1 cm above hood top at (x, y, z) = (0, 59, 136) cm

H (cm)	V_s (ms^{-1})	C_{ave} (ppm)
3	4	0.001
	8	<0.001
	12	<0.001
25	4	0.009
	8	<0.001
	12	<0.001
50	4	0.037
	8	0.018
	12	<0.001

T_{plate}=220°C, v_b=1 ms^{-1}.

(V_s=8 and 12 m/s), the measured SF_6 concentrations are less than 0.001 ppm (which means "non-detectable"). At H=25 cm, C_{ave} of the SF_6 concentration at V_s=4 m/s becomes a little larger (0.009 ppm) when compared with its counterpart of H=3 cm. At higher suction velocities (V_s=8 and 12 m/s), C_{ave} of SF_6 concentrations are less than 0.001 ppm. At the large sash opening H=50 cm, the values of C_{ave} become large—0.037 and 0.018 ppm for V_s=4 and 8 m/s, respectively. While the measured SF_6 concentrations are still less than 0.001 ppm at V_s=12 m/s. Comparing the results of Table 1 with the flow visualization results shown in Figs. 9 and 10, it is apparent that the quantitative measurements of SF_6 concentration at the location above the hood top closely correlate with the results of flow visualization. If the maximum height H_m shown in Figs. 9 and 10 are below the hood-top level (the upper dashed line), no SF_6 leakage is observed. As the maximum height H_m shown in Figs. 9 and 10 are near or beyond the hood-top level, SF_6 concentrations are detected. According to Table 1 and Figs. 9 and 10, at high temperature operation of the air-curtain fume hood the suction velocity V_s and the sash height H must be adjusted in the safe regime.

Conclusions

The flow and leakage characteristics of the air-curtain fume hood under high temperature operation (between 100°C and 250°C) were studied. The primary parameters dominating the behavior of the flow field and hood performance are the sash height, suction velocity, and operation temperature. In general, at large sash height and low suction velocity, the air curtain breaks down to present a severely concave mode and strong three-dimensional flow is induced in the cabinet, therefore containment leakage from the sash opening is observed. Since the suction velocity is low and the sash opening is large, the makeup air quantity drawn from the hood top becomes less. The hot plume therefore has less ability of counter acting the down flow and rises beyond the hood top. At small sash opening and high suction velocity, the air curtain presents the slight concave mode and the flow in the cabinet behaves less three dimensional. Because the air curtain is robust and the makeup air flow is sufficiently large under this situation, the containment leakages from the sash opening and the hood top are not observed. If the operation temperature is between 100°C and 200°C, setting the sash height to be smaller than 25 cm is able to obtain negligible leakage at a medium suction velocity of 8 m/s. If the sash height is 50 cm, the suction velocity has to increase to values beyond 12 m/s to confine the hot plume below the half cabinet height. If the operation temperature is between 200°C and 250°C the sash height should not be larger than 25 cm and the suction velocity should not be less than 12 m/s.

References

1) Ahn K, Woskie S, DiBerardins L, Ellenbecker M (2008) A review of published quantitative experimental studies on factors affecting laboratory fume hood performance. J Occup Environ Hyg **5**, 735–53.
2) First MW (2003) Laboratory chemical hoods: a historical perspective. AIHA J **64**, 251–9.
3) Ivany RE, First MW, Diberardinis LJ (1989) A new method for quantitative, in-use testing of laboratory fume hoods. Am Ind Hyg Assoc J **50**, 275–80.
4) Fletcher B, Johnson AE (1992) Containment testing of fume hoods - I methods. Ann Occup Hyg **36**, 239–52.
5) Fletcher B, Johnson AE (1992) Containment testing of fume hoods - II test room measurements. Ann Occup Hyg **36**, 395–405.
6) Saunders T (1993) Laboratory Fume Hoods: A User's Manual, 56–81, John Wiley & Sons, New York.
7) Volin CE, Joao RV, Reiman JS, Party E, Gershey EL (1998) Fume hood performance: face velocity variability inconsistent air volume systems. Appl Occup Environ Hyg **13**, 656–62.
8) Maupins K, Hitchings DT (1998) Reducing employee exposure potential using the ANSI/ASHRAE 110 Method of Testing Performance of Laboratory Fume Hoods as a diagnostic tool. Am Ind Hyg Assoc J **59**, 133–8.
9) Ekberg LE, Melin J (2000) Required response time for variable air volume fume hood controller. Ann Occup Hyg **44**, 143–50.
10) Flynn MR, Ljungqvist B (1995) A review of wake effects on worker exposure. Ann Occup Hyg **39**, 211–21.
11) Guffey SE, Flanagan ME, van Belle G (2001) Air sampling

at the chest and ear as representative of the breathing zone. Am Ind Hyg Assoc J **62**, 416–27.
12) Tseng LC, Huang RF, Chen CC, Chang CP (2006) Correlation between airflow patterns and performance of a laboratory fume hood. J Occup Environ Hyg **3**, 694–706.
13) Tseng LC, Huang RF, Chen CC, Chang CP (2007) Aerodynamics and performance verifications of test methods for laboratory fume cupboards. Ann Occup Hyg **51**, 173–87.
14) Bennett JS, Crouch KG, Shulman SA (2003) Control of wake-induced exposure using an interrupted oscillating jet. Am Ind Hyg Assoc J **64**, 24–9.
15) Ekberg LE, Melin J (2000) Required response time for variable air volume fume hood controllers. Ann Occup Hyg **44**, 143–50.
16) Huang RF, Wu YD, Chen HD, Chen CC, Chen CW, Chang CP, Shih TS (2007) Development and evaluation of air curtain fume cabinet with its considerations of aerodynamics. Ann Occup Hyg **51**, 189–206.
17) Huang RF, Chen HD, Hung CH (2007) Effects of walk-by and sash movement on aerodynamics and contaminant leakage of air curtain-isolated fume hood. Ind Health **45**, 804–16.
18) Huang RF, Lin SY, Jan SY, Hsieh RH, Chen YK, Chen CW, The WY, Chang CP, Shih TS, Chen CC (2005) Aerodynamic characteristics and design guidelines of push-pull ventilation systems. Ann Occup Hyg **49**, 1–15.
19) European Committee for Standardization (2003) EN: 14175-3: 2003 Fume cupboards-Parts 3: type test methods. European Committee for Standardization, Brussels.
20) American Society of Heating, Refrigeration and Air Conditioning Engineers Inc (1995) ANSI/ASHRAE Standard 110–1995: Method of testing performance of laboratory fume hoods. American Society of Heating, Refrigeration and Air Conditioning Engineers Inc. Atlanta.
21) Tsai SJ, Huang RF, Ellenbecker MJ (2010) Airborne nanoparticle exposures while using constant-flow, constant-velocity, and air-curtain isolated fume hoods. Ann Occup Hyg **54**, 78–87.
22) Tsai SJ, Ada E, Isaacs J, Ellenbecker MJ (2009) Airborne nanoparticle exposures associated with the manual handling of nanoalumina and nanosilver in fume hoods. J Nanopart Res **11**, 147–61.
23) Flagan RC, Seinfeld JH (1988) Fundamentals of Air Pollution Engineering, 290–357, Prentice Hall, Englewood Cliffs, New Jersey.